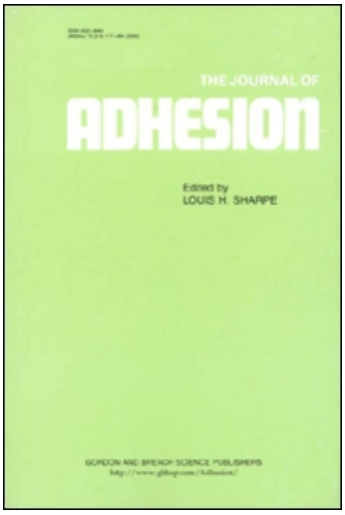

The Journal of Adhesion
Publication details, including instructions for authors and subscription information:
http://www.informaworld.com/smpp/title~content=t713453635

XPS of the Interphase Between PMMA and Metals. A Study of Degradation and Interaction

Wulff Possart[a]; Volker Schlett[b]
[a] Aussenstelle Teltow, Fraunhofer-Institut für Angewandte Materialforschung, tow, Germany [b] Fraunhofer-Institut für Angewandte Materialforschung, Bremen (Lesum), Germany

To cite this Article Possart, Wulff and Schlett, Volker(1995) 'XPS of the Interphase Between PMMA and Metals. A Study of Degradation and Interaction', The Journal of Adhesion, 48: 1, 25 — 46
To link to this Article: DOI: 10.1080/00218469508028152
URL: http://dx.doi.org/10.1080/00218469508028152

J. Adhesion, 1995, Vol. 48, pp. 25–46
Reprints available directly from the publisher
Photocopying permitted by license only

XPS of the Interphase Between PMMA and Metals. A Study of Degradation and Interaction*

WULFF POSSART**

Fraunhofer-Institut für Angewandte Materialforschung, Aussenstelle Teltow, Kantstraße 55, D-14513 Teltow, Germany

and

VOLKER SCHLETT

Fraunhofer-Institut für Angewandte Materialforschung, Lesumer Heerstrass 36, D-28717 Bremen (Lesum), Germany

(Received March 27, 1993; in final form April 15, 1994)

XPS was applied to PMMA layers of varying thickness in the nanometer range on gold and natural aluminium surfaces, respectively. The numerical decomposition of the core levels into the contributions from the various atomic bonding states reveals some peculiar features of the interphase region to the metals. First, for both metals special mechanisms of thermal destruction are deduced. On Au the splitting of complete methacrylate side groups and, even more intense, the stripping of (—O—CH_3)-units is found while on Al the side group scission is verified only. Secondly, the metals reveal different effects on the electron density in the methacrylate groups. Au appears to be inert but the natural Al surface exerts a withdrawing effect on the electrons of both the carbon and the oxygen atoms in the side groups.

KEY WORDS XPS; polymer-metal interphase; thermal destruction; adhesive interactions; PMMA; gold; aluminium.

INTRODUCTION

As a well established means, XPS investigations have been applied to a great number of problems on polymer science, surface chemistry of polymers and adhesion for a long time. In context with the characterization of polymer-metal interphases in general, and adhesion properties in particular, the *in-situ* investigation of the contact is necessary. Due to the limited information depth as a surface sensitive method, XPS requires special preparation techniques to meet this aim. There are three different ways reported in the literature. First, stepwise evaporation of metal onto a polymer substrate provides

*Presented at the European Adhesion Conference EURADH'92, September 21–24, 1992, in Karlsruhe, Germany.

**Corresponding author.

interesting insight, *e.g.*, Refs. 1–9. But the interaction of hot metal atoms with a polymer surface in vacuum certainly differs from the interaction between a metal surface and macromolecules put on it from a solution. Second, an inspection of the polymer-metal interface through the metal requires a very special and cumbersome preparation.[10] Third, another appropriate and not too complicated way consists in the formation of thin films with varying thickness on the metallic substrate.[11–15] The latter idea is applied in this work since it seems to be closest to real conditions of adhesive contact formation. Particularly, we use the polymer thickness variation as a means of changing the ratio of contributions from the bulk and the interphase regions to the photoelectron spectra in the range of thin coatings.

Unfortunately, real adhesive interphases are too complex for basic research needs due to the numerous components and environmental influences involved. Looking for some model system, we found PMMA to be quite an appropriate model polymer. Its macromolecules contain methacrylate side groups which may serve as a model atom group for the class of acrylic adhesives. Moreover, PMMA has been well studied by XPS, *e.g.* Refs. 16–21. With respect to the metal, industrially manufactured surfaces are very complex systems also. Therefore, we chose evaporated metal surfaces on silicon wafers as model substrates.

With these model systems, XPS investigations were performed in order to find out what information the core level spectra provide and what has to be added in order to establish the correlation with the properties of the polymer-metal interphase. The paper starts with the experimentally established state of the core electrons of carbon and oxygen in the surface region of thick PMMA layers and with the bonding state of the characteristic metal electron levels on the uncoated substrates. Then the corresponding XPS spectra are considered as they change with the thickness of the PMMA layer on Al and Au, respectively. This discussion is based on the decomposition of the photo lines into spectral components which reflect the binding state of the considered element *via* its core electron binding energy, BE. The results are interpreted in terms of peculiar steps of polymer thermal destruction and of a modification of the bond state in those polymer side groups on which the substrate exerts a particular influence.

EXPERIMENTAL

Due to their surface finish, polished silicon wafers are excellent substrates for evaporated thin metal films. Optically flat gold or aluminium layers of about 1 μm thickness were thermally evaporated on the wafers by resistance heating in a high vacuum chamber equipped with a water-cooled baffle.

PMMA ($\bar{M}_n \approx 5 \cdot 10^4$) was produced by free radical polymerization, precipitated twice for cleaning and dissolved in freshly distilled acetone (polymer concentration range 0.1–3 weight %). Spin casting of these solutions, under laboratory atmosphere, at room temperature and 5000 rpm provided PMMA films of various thickness on top of the metal layers.

The polymer thickness was measured with the help of an ellipsometer using the optical constants of the substrate determined prior to coating and by assuming that the PMMA forms a homogeneous transparent film. Thus, the calculated polymer thick-

ness d(Elli) is an average over the laser spot area (∅ *ca.*1 mm). The mean values of at least ten measurements at different positions across the sample prove a fairly uniform film thickness with statistical errors ranging from about 1% for the thick layers to not more than 10% for the 3 nm layers. This result confirms the assumed homogeneity and continuity of the film at least on the macroscopic scale of sample area.

Core level photo electron spectra were recorded for all samples on a VG ESCALAB MK2 in the CAE mode applying MgK_{α}X-rays, 0° take-off angle, 10 eV pass energy, and a chamber pressure of less than $2 \cdot 10^{-8}$ Pa. The X-ray tube was run at either 240 W or 60 W in order to minimize the X-ray exposure of the PMMA.

In order to obtain some insight into possible radiation damage, the series of carbon and oxygen spectra was measured twice for each of the PMMA layers on gold at the selected value of X-ray tube power. Therefore, the C1s-and O1s-spectra from the first measuring sequence represent the polymer state after shorter X-ray exposure than the corresponding spectra from the second sequence of measurement. The radition damage can be estimated by comparing these two sequences of spectra.

For spectral decomposition, our own software package[22] was employed in the following manner. After a base line correction by a generalized Tougaard background, a sum of k components with the line shape function $f(E)$ proposed by Hughes and Sexton[23] are fitted *via* a damped least square algorithm:

$$f(E) = \sum_{k} \frac{I_{0,k} \exp[-\ln(2)(1-M)B_k]}{(1 + M B_k)}$$

with

$$B_k = \frac{(E - E_{\max,k})^2}{(Z \beta_k)^2}$$

$$Z = A_0 + A_1 M + A_2 M^2 + A_3 M^3 + A_4 M^4 + A_5 M^5 + A_6 M^6$$

A_i = numerical constants $i = 1 \cdots 6$
I_0 = peak height
$E_{\max}$ = kinetic energy at peak maximum
β = half width at half maximum
M = Gauss-Lorentz mixing ratio

Figures 1 and 2 illustrate the typical results of the fitting procedure for a C1s-and a O1s-core level spectra of PMMA, as an example. In both examples, the sum of components fits the experimental curve well. Further proof for the validity of our algorithm is given with the results for bulk-like PMMA.

RESULTS AND DISCUSSION

PMMA Spectra

PMMA and other polymethacrylates have been the subject of careful studies which have provided detailed knowledge about the fine structure of their photoelectron spectra. The work of Pijpers, Donners and Meier[16-18] and further investigations, *e.g.*, Refs. 19–21, led to the conclusion that the C1s photo line of PMMA consists of four

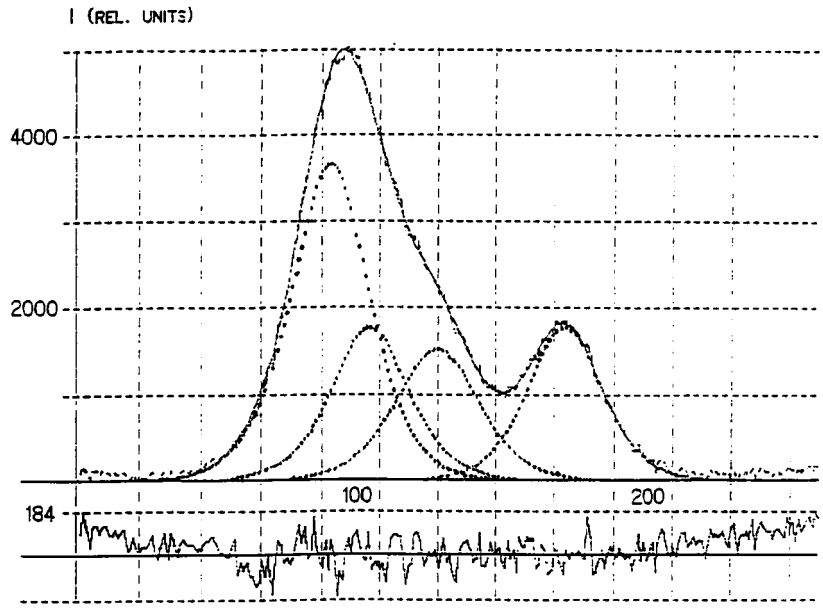

FIGURE 1 High resolution C1 spectrum of 42.6 nm PMMA on gold. The binding energy is given in channels of 0.05 eV distance on the x-axis. --- = raw data; — = convolution of the fit; ··· = fitted components. The curve in the diagram below the spectrum shows the corresponding residues as a measure for the goodness of the fit.

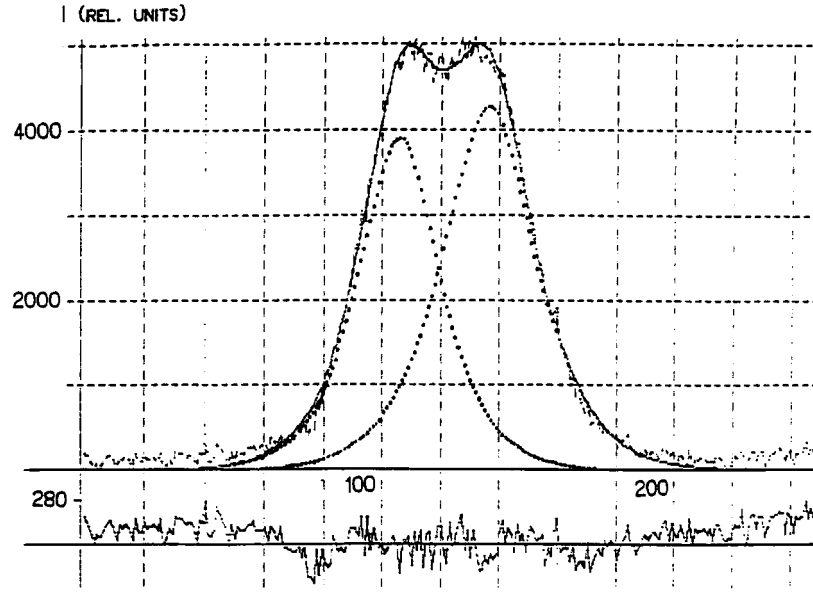

FIGURE 2 High resolution O1 s spectrum of 42.6 nm PMMA on gold as for Figure 1.

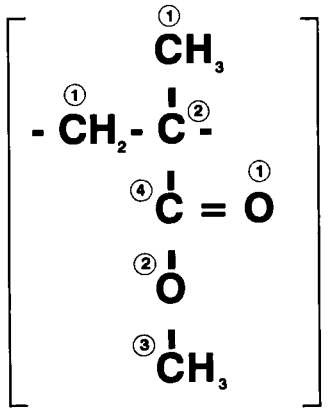

FIGURE 3 Monomer unit of PMMA with the different bond states enumerated at the atoms.

components corresponding to the chemical composition given in Figure 3: The aliphatic bonded **C1**, the aliphatic bonding state **C2** which is shifted to higher binding energies due to the next-nearest oxygen influence (so-called β-shift), the bonding state **C3** influenced by the carboxyl group, and finally the state **C4** of the carbonyl carbon. With these presuppositions all C1s spectra of the polymer films in this work are fitted by four components.

In accordance with the PMMA structure, the O1s spectra are fitted by two components representing the carbonyl and the ether oxygen, respectively. (For some peculiarities with thin PMMA films on Al see the thin layers on Al).

Table I summarizes our results for the spectra deconvolution for thick PMMA films on gold and aluminium. The effect of a minor sample charging on the binding energies is depicted by the absolute BE values for C1 which should be about 285 eV on uncharged samples. For the remaining C1s and O1s components the charge shift is eliminated by referencing their peak position to the corresponding BE(C1). These relative peak positions ΔBE are equal for both films and they are also in full accordance with published data.[17,18,20,21] Therefore, it is inferred that our peak deconvolution algorithm works well. As for the literature data, the component intensity ratios do not meet exactly the expected stoichiometric ratios (C1:C2:C3:C4 = 2:1:1:1 and O1:O2 = 1:1) on gold. The effect is not fully explained yet, although several proposals have been made in the literature. For example, the underestimated relative intensities of C4 and O1 may be attributed to some shake up/shake off phenomena correlated with the π-bond in (C=O).[19-21] For the thick PMMA layer on the aluminium substrate, the relative intensities of C3, C4 and,hence, of C2 in the methacrylate group are lower than on gold. This could indicate some depletion of methacrylate groups in the surface region of the PMMA on aluminium.

Hence, our results reproduce for thick films just the expected binding states of bulk PMMA and are suited as reference data for the discussion of the thin film properties.

TABLE I
Fit results for thick PMMA layers at 240 W X-ray tube power

	PMMA	42.6 nm on Au	44 mm on Al
	BE[eV]	286.69	287.50
C1	rel. HWHM[a]	1.07	1.07
	I_{int}[b]	2000	2000
	ΔBE[c][eV]	0.71	0.72
C2	rel. HWHM[a]	1.07	1.07
	rel. I_{int}[d]	972	822
	ΔBE[c][eV]	1.85	1.84
C3	rel. HWHM[a]	1.13	1.13
	rel. I_{int}[d]	864	785
	ΔBE[c][eV]	4.03	4.01
C4	HWHM[e]	1	1
	rel. I_{int}[d]	912	768
	ΔBE[c][eV]	247.17	247.13
O1	rel. HWHM[f]	0.89	0.87
	I_{int}[g]	1000	1000
	ΔBE[c][eV]	248.72	248.67
O2	HWHM[e]	1	1
	rel. I_{int}[h]	1220	1237

[a] HWHM relative to HWHM(C4); [b] set to 2000 relative units; [c] BE-difference to BE(C1); [d] I_{int} relative to I_{int}(C1); [e] set to 1 relative unit; [f] HWHM relative to HWHM(O2); [g] set to 1000 relative units; [h] I_{int} relative to I_{int}(O1).

Substrate Spectra

Two components are taken to fit the spin-orbit split Au4f photo lines. These lines are not only observed for the uncoated substrate but also through the thin PMMA layers (Figure 5). From the literature,[25] reference value of (84.00 ± 0.01) eV is expected for the binding energy of $Au4f_{7/2}$. Our measurements provide (84.12 ± 0.02) eV for this line position. Hence, the chemical state of the gold layer can be considred as purely elemental. As is usual for metals, the bare gold surface is covered by an adventitious carbon-based contamination. The C1s signal consists of a single peak with an asymmetric tail at the high binding energy side-see Figure 4a. A thickness of *ca.* 2.5 nm is estimated from the XPS intensity. The consequences of this contamination for the interpretation of the photoelectron spectra for the thin PMMA films will be discussed in the Appendix.

On the bare Au substrate a distinct O1s signal was observed. It consists of a broad line at 532.4 eV (HWHM $\approx$ 1.16 eV) with an asymmetric tail on the low binding energy side. Probably this photo line can be attributed to adsorbed water, which causes similar spectral features due to its various adsorbtion states.[28,29]

As expected, thin oxide films form of top of the aluminium in contact with the laboratory atmosphere. Therefore, the Al2p spectrum consists of two components. The binding energy of the metallic component $[BE(Al^0) = (72.91 \pm 0.01)$ eV] agrees well with the corresponding literature data.[30-35] In our spectra, the non-metallic Al2p component has a binding energy, BE = (75.58 ± 0.01) eV. This is just 2.67 eV above the metal state. Fritsche *et al.*[32], and especially Evans *et al.*[36], concluded from well-controlled oxidation experiments in vacuo that the Al2p photo line should be

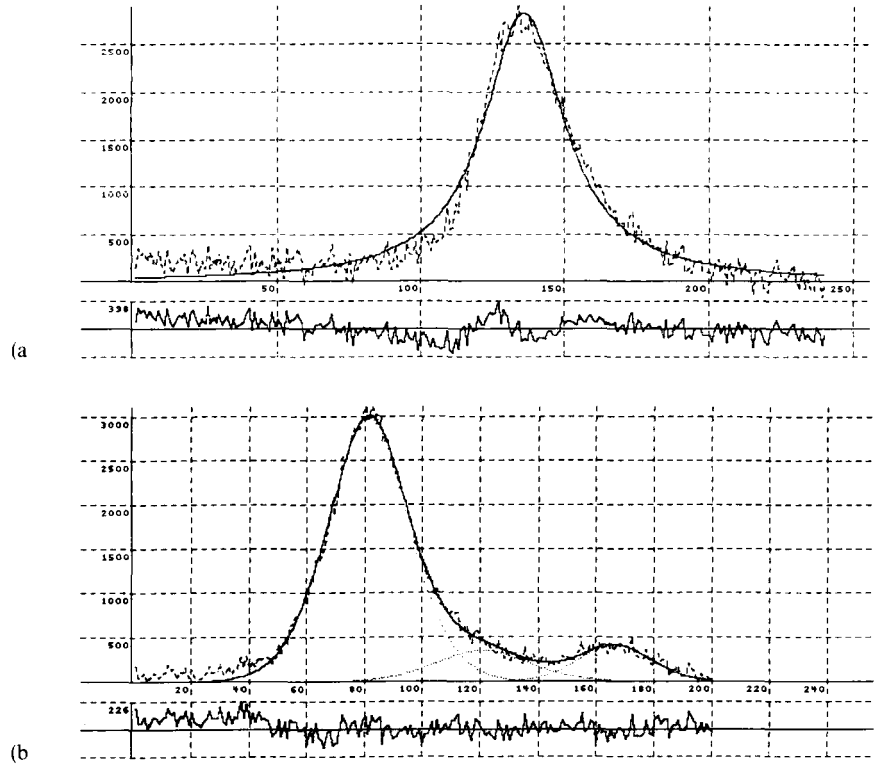

FIGURE 4 C1s spectra of the carbon contamination on the bare substrate surfaces. a) gold, fitted by one component; b) aluminium, fitted by three components.

2.4–2.5 eV above the binding energy of the pure metal for the oxide state and 2.66–2.77 eV in the case of the hydroxide. Hence, the position of the second Al2p component in our spectra indicates a pronounced hydroxide content for the oxide films which can be considered as the native surface layer of the Al that is in contact with the deposited PMMA.

The strong O1s signal of the uncoated Al substrate is composed of two components with BE = 532.26 eV and BE = 533.39 eV. Due to the reported data,[34,36,37] and in accordance with the Al2p components, these peaks are attributed mainly to the oxygen in aluminium oxide and hydroxide, respectively. An oxide layer thickness of about 2–3 nm is deduced from both XPS and ellipsometric measurements.

Again, the Al substrate surface is contaminated by *ca.* 1.5 nm carbon compounds. However, the C1s spectra consists of three components, see Figure 4b. Their binding energies resemble PMMA but much less intensity is distributed on the (C—O—)- and the (C=)-like bonds in the contamination. Since the Al surface is formed by the same preparation steps as the gold layer, the two additional C1s bond states in the carbon contamination seem to be a peculiar feature of the oxidized aluminium surface. As is discussed in the Appendix, this contamination is probably not present beneath the PMMA films.

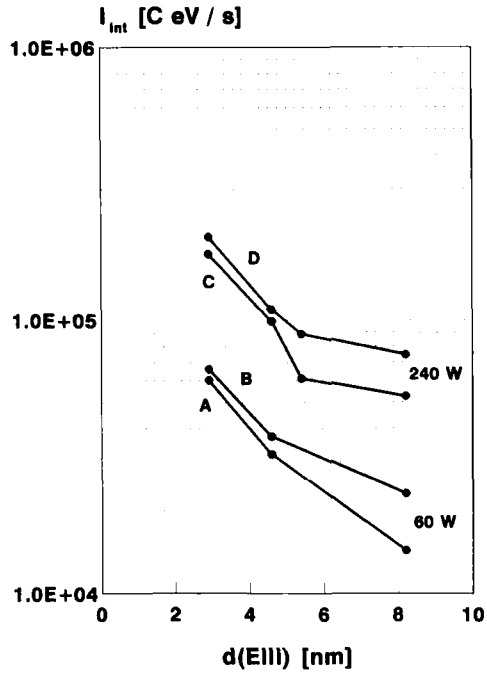

FIGURE 5 Gross integrated intensity I_{int} for the Au4f spectra as a function of PMMA thickness, d(Elli). Curves A and C depict the I_{int} measured with the 1st sequence of spectra while curves B and D give the data for the 2nd sequence (*i.e* prolonged X-ray exposure).

For the thin PMMA layers, Figure 5 shows the expected decline in the Au4f line intensity with rising polymer thickness d(Elli). Curves A and C summarize the data obtained in the first sequence of measuring the C1s, the O1s, and the Au4f spectra of the coated samples (cf. Sect. 2). As expected, the increased X-ray tube power for Curve C results in an enhanced signal intensity level compared with curve A. Curves B and D are derived from the Au4f spectra measured in a second sequence on the same samples with the denoted power values. Obviously, both curves are systematically shifted to a higher intensity level with respect to the first sequence of measurement. This is caused by a reduction of the polymer film thickness due to some degradation mechanism. The thickness reduction is estimated as follows.

Assuming a homogeneous layer with the thickness d_P of a material P on top of the gold substrate, the integral photo line intensity I(Au4f) for Au can be calculated as:[26]

$$I(\mathrm{Au}4f) = I^{\infty}(\mathrm{Au}4f)\exp\left\{-\frac{d_P}{\delta_P(E_{\mathrm{Au}})\cos\theta}\right\} \tag{1}$$

I^{∞}(Au4f) = integral photo electron intensity from the pure semi-infinite gold substrate
$\delta_P(E_{\mathrm{Au}}) = e^-$ escape depth (in some length unit) of the Au4f electrons in the material P
θ = take-off angle of the photo electrons; here 0°.

TABLE II
Reduction of PMMA thickness on gold as a function of X-ray exposure. All data in nm. The polymer thickness *d*(Elli) is measured by an ellipsometer

d(Elli)	2.9	4.6	5.4	8.2
$-\Delta$dp(60 W)	0.31	0.52	—	1.97
$-\Delta$dp(240 W)	0.50	0.34	1.54	1.34

For organic materials, δ may be estimated from the equation[27]

$$\delta(E) = 49 \cdot E^{-2} + 0.11 \cdot E^{0.5} \tag{2}$$

where E is the kinetic energy in eV and δ the escape depth of the electrons (here in $mg \cdot m^{-2}$ according to Ref. 27). Dividing the result of Equation (2) by the density of PMMA (*ca.* $1.18\,g \cdot cm^{-3}$) provides $\delta_P(\text{Au}4f) \approx 3.19$ nm. Differentiation of Equation (1) yields

$$\Delta d_P = -\delta_P(E_{\text{Au}4f}) \frac{\Delta I(\text{Au}4f)}{I(\text{Au}4f)} \tag{3}$$

Table II summarizes the polymer thickness reduction ($-\Delta d_P$) as calculated from Equation (3) and the Au4*f* intensity rise from curve A to curve B and from curve C to curve D in Figure 5. Although the Δd_P data scatter considerably, the partial destruction is obvious for all films.

For explanation we stress that the thicker films lose more material on an absolute scale than the thinner ones for the *same* X-ray dose (see Table II). In fact, the PMMA possesses poor heat conductivity. The thicker films reach higher temperatures under the heat radiation from the hot nose of the X-ray tube than the thinner films, even for the chosen 25 mm distance between X-ray source and sample surface. In turn, this temperature rise produces growing rates of *thermal* destruction with rising PMMA thickness. The X-ray photon flux density cannot be blamed for the thickness loss since it remains nearly constant in all of these thin polymer layers. As a third possible reason, the Au4f photoelectrons could cause electron-induced damage to the polymer molecules. This effect may be neglected here since it should produce more thickness reduction in the thin films than in the thicker ones. Table II reveals the opposite. All this indicates that the destruction of the PMMA film is mainly caused by a temperature increase and not by radiation damage.

A comparison of our conclusions with the literature, *e.g.* Refs. 44–47, is not straightforward since the X-ray doses are not given explicitly there. So with ordinary polychromatic Al K_α X-rays, the picture is quite confusing but some effect of temperature on the destruction of bulk PMMA is at least indicated.[46] This view is also supported by the work of Buchwalter and Czorny[47] who state a reduction of molecular weight, but no loss of material, for bulk PMMA under the irradiation with a monochromatized AlK_α source where temperature load at the sample is avoided.

Thin PMMA Films

Thin Layers on Gold As is shown in the Appendix, the carbon contamination should be absent at the interface between gold and PMMA. Therefore, the features of the C1s spectra can be attributed directly to the polymer films.

Figure 6 depicts the integral intensities of the whole C1s signal recorded at the fresh PMMA layers (first measuring sequence according to Sect. Experimental) and its four components as a function of polymer thickness. Obviously, the fractions of the methyl group bonded to the ether oxygen (component **C3**) decreases steeper with the film thickness than the fraction of the other carbon species (**C1, C2,** and **C4**). Table III summarizes these data for all measurements on gold. Comparing the first with the second sequence of measurement, the $C1/C_{int}$ ratios for corresponding polymer thickness clearly prove the tendency of a growing aliphatic C1s signal with increasing exposure time. The effect is more pronounced for the 240 W than for 60 W X-ray tube power. In any case, it amounts to only a few per cent of the gross signal intensity. Hence, most of the polymer retains the original chemical composition. Simultaneous to the increasing $C1/C_{int}$ ratio, a time-dependent reduction of both the C3 and the C4 in the methacrylate groups relative to C1 can be stated (compare the data for C3/C1 and for C4/C1 in Table III). Not only do these findings confirm the general conclusion drawn above from the metal photo lines about the thermal destruction of PMMA during

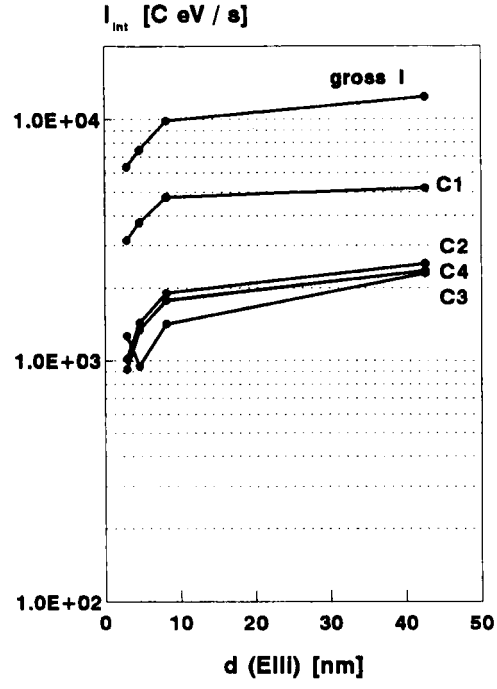

FIGURE 6 Gross integrated intensity of the C1 s signal and its components C1, C2, C3, and C4 for PMMA on gold. 1st sequence at 60 W X-ray tube power.

TABLE III
Relative intensity of the Cls components for PMMA on gold

d(Elli) [nm]	60 W X-ray tube power							
	1. sequence				2. sequence			
	$\frac{C1}{C_{int}}$	$\frac{C3}{C1}$	$\frac{C4}{C1}$	$\frac{C3}{C4}$	$\frac{C1}{C_{int}}$	$\frac{C3}{C1}$	$\frac{C4}{C1}$	$\frac{C3}{C4}$
2.9	0.496	0.402	0.292	1.377	0.550	0.232	0.279	0.831
4.6	0.501	0.253	0.360	0.704	0.532	0.243	0.174	0.791
8.2	0.483	0.298	0.373	0.799	0.512	0.250	0.339	0.736
42.6	0.421	0.443	0.454	0.975	—	—	—	—
280.2	0.434	0.423	0.425	0.995	—	—	—	—

d(Elli) [nm]	240 W X-ray tube power							
	1. sequence				2. sequence			
	$\frac{C1}{C_{int}}$	$\frac{C3}{C1}$	$\frac{C4}{C1}$	$\frac{C3}{C4}$	$\frac{C1}{C_{int}}$	$\frac{C3}{C1}$	$\frac{C4}{C1}$	$\frac{C3}{C4}$
2.9	0.527	0.226	0.330	0.684	0.526	0.305	0.290	1.053
4.6	0.512	0.260	0.338	0.768	0.585	0.194	0.250	0.778
5.4	0.464	0.353	0.388	0.912	0.526	0.308	0.286	1.076
8.2	0.455	0.347	0.412	0.841	0.532	0.279	0.291	0.961
42.6	0.421	0.432	0.456	0.947	0.525	0.293	0.296	0.988

measurement. The enhanced depletion of the species C3 and C4 (representing the methacrylate side groups) also demonstrates that the decomposition process of thin PMMA films in contact with gold is not confined to a simple depolymerization as is described for bulk material in the literature.[38-43] On the contrary, methacrylate groups preferentially split off from the backbone. Note that only a small part of the macromolecules is subjected to this specific destruction. The mechanism is more obvious for the thinner films and may possibly occur in a certain narrow boundary layer near the interface with the gold.

Another peculiarity appears for the C3/C4 ratio, especially for the first measuring sequence, see Table III. With decreasing polymer thickness, this ratio shifts to smaller values and remains almost constant during the second sequence. That indicates the stripping of ($-O-CH_3$) fragments as an additional destruction process which is even faster than the splitting of complete methacrylate groups in the thin films.

A consideration of the O1s signal will confirm these conclusions. Figure 7 depicts the integral intensity of the total O1s signal for all four measured series of spectra as a function of polymer thickness. Due to the polymer decomposition, the loss of signal intensity with growing exposure time (from curve I to curve II and from curve III to curve IV) is quite obvious for 240 W as well as for 60 W X-ray tube power. It is worth noting that the integral intensity decreases even for the very thin films, though

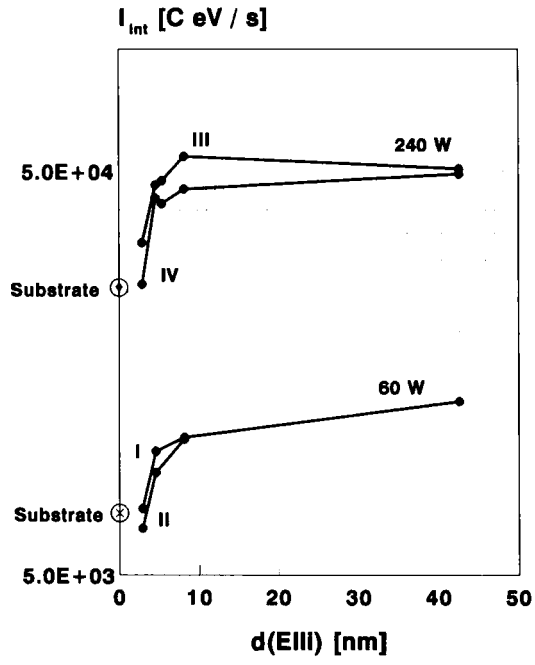

FIGURE 7 Gross integrated intensity of O1 s as a function of PMMA thickness on gold. I, III = 1st sequence and II, IV = 2nd sequence for 60 W and 240 W X-ray tube power, respectively. The intensity values for O1 s on the bare Au are indicated on the ordinate.

comparable O1s signal intensities have been recorded on the bare gold (see the marks on the ordinate in Figure 7). In Section 3.2, the O1s signal on bare Au has been attributed to adsorbed water. It should provide a significant contribution to the O1s signal for the coated samples as well if the adsorbed water layer would have been buried under the polymer. Evidently this is not the case for the curves in Figure 7.

The ratio of the two oxygen components O1 (carbonylic) and O2 (ether-like) is included in Table IV for both values of X-ray power. Due to their strong overlap, the intensity data of the decomposed O1s components are less certain than those of the C1s

TABLE IV
Relative intensity O2/O1 for the two O1s components of PMMA on gold

d(Elli) [nm]	60 W		240 W	
	1. sequence	2. sequence	1. sequence	2. sequence
2.9	0.650	1.103	1.311	0.877
4.6	0.548	0.596	0.390	0.479
5.4	—	—	1.243	1.044
8.2	0.825	1.330	0.985	1.189
42.6	1.256	—	1.220	1.297
280.2	1.146	—	—	—

spectra. Hence, tendencies are less pronounced in Table IV. Nevertheless, the O2/O1 ratio decreases with polymer thickness for the first sequence at 60 W and for the second sequence at 240 W, as it should be if the ($-O-CH_3$) units split off faster than complete methacrylate groups in thin PMMA layers.

As stated above, the peculiar thermal destruction processes affect only a small portion of PMMA molecules. This is also confirmed by the core level photoelectron spectra obtained for all polymer layers. They are very similar to those of the bulk PMMA and no line components have been resolved which could be ascribed to bond states resulting from the side group destruction. Therefore, the line positions in the spectra are attributed to the remaining intact macromolecules.

In Figures 8a and b the peak positions of the components are referred to the binding energy of the component C1. This referencing eliminates the sample charging effects from consideration. The binding energies of all C1s and O1s components of PMMA reproduce the data of the bulk state within a certain scatter. They do not depend on the polymer thickness. Hence, the gold does not exert a detectable interfacial interaction on the bond state in the intact PMMA molecules.

Thin Layers on Aluminium As shown in Figure 9a, on aluminium the aliphatic component C1 of the C1s photo line decreases only slowly with decreasing polymer thickness, at the expense of the methacrylate group components C2, C3, and C4 which lose intensity quite strongly below ca. 10 nm. In the Appendix it is shown that there is again no carbon contamination detected under the PMMA. As for the gold substrates, splitting of methacrylate side groups appears, therefore, as the peculiar destruction process for the thin PMMA films on aluminium.

This conclusion also becomes obvious from Table V. Moreover, the ratio C3/C4 does not depend on polymer thickness here. Hence, in contrast to the findings for gold substrates, the peculiar destruction mechanism on Al is confined to the stripping of complete side groups from the PMMA backbone. No extra splitting of ($-O-CH_3$) groups occurs on aluminium.

Figure 9b depicts the gross and component intensities of O1s as a function of film thickness. In contrast to the situation on gold (Fig. 7), the gross O1s intensity rises with decreasing film thickness due to the contribution from the aluminium oxide. Moreover, we found the binding energy of the O1s from the aluminium hydroxide to be just equal to that of the charge-shifted O1 component of the carbonyl oxygen in the thin polymer films. This signal interference causes the intensity rise of the O1 component with decreasing film thickness in Figure 9b. Hence, the O2/O1 ratio cannot be discussed in context with polymer thickness on aluminium. However, the intensity decline of the undisturbed O2 component (Fig. 9b) confirms, once more, that thin films (*i.e.*, a those with a large interphase content) decompose *via* the splitting of methacrylate side groups-a process which does not occur in bulk PMMA .

Figure 10a, b provide the energy differences ΔBE of the C1s and the O1s components as referred to the aliphatic carbon C1 ($BE = 284.8$ eV). These ΔBE curves are not influenced by sample charging. As discussed for gold, we do not resolve additional bond states due to the small amount of destroyed macromolecules in the core electron spectra. Hence, the curves in Figure 10 depict the relative photo electron binding energies of atoms in the intact methacrylate side groups. On aluminium, the ΔBE

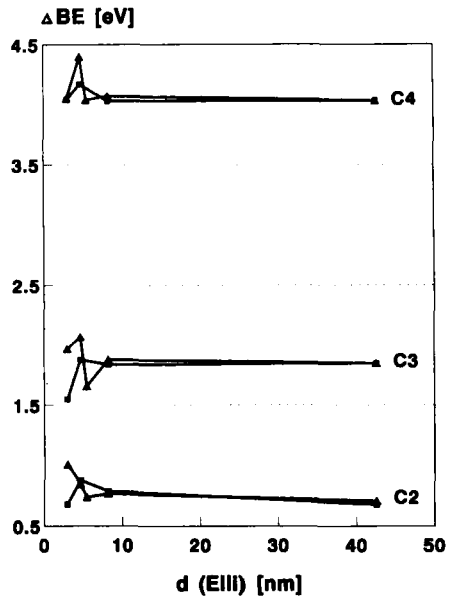

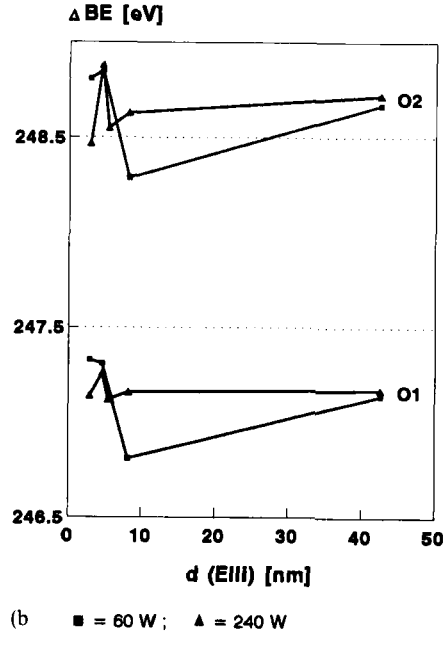

FIGURE 8 Relative binding energies ΔBE for the C1 s components (a) and the O1 s components (b) of PMMA as a function of polymer thickness on gold.

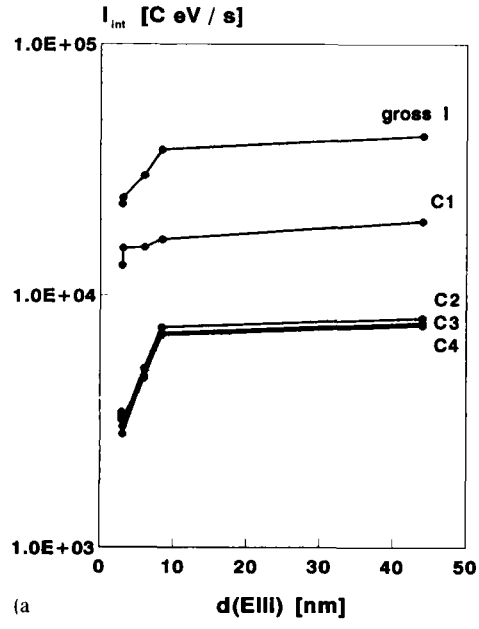

(a

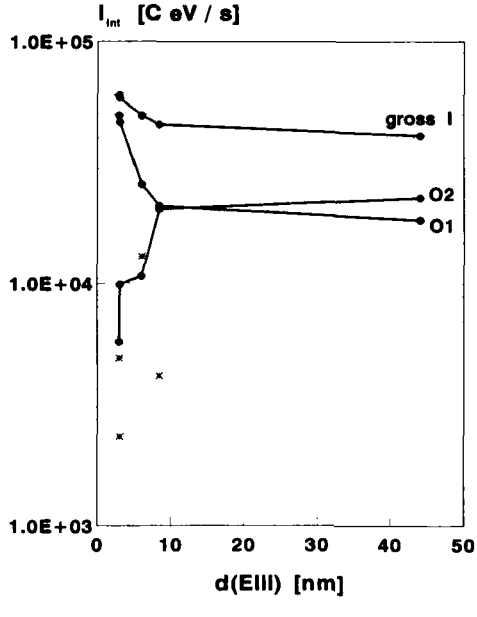

(b * = O in oxyd. Al

FIGURE 9 a) Gross integrated intensity of C1 s and its components C1, C2, C3, and C4 for PMMA on aluminium. b) Gross integrated intensity of O1 s and its components O1, and O2 for PMMA on aluminium. *** = oxygen in oxidized Al as determined beneath the PMMA coating.

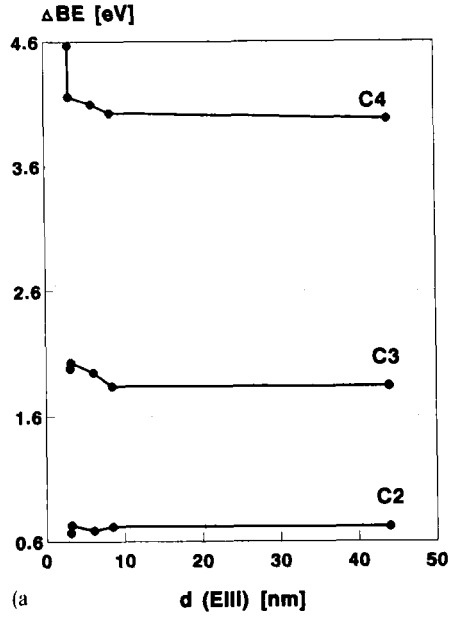

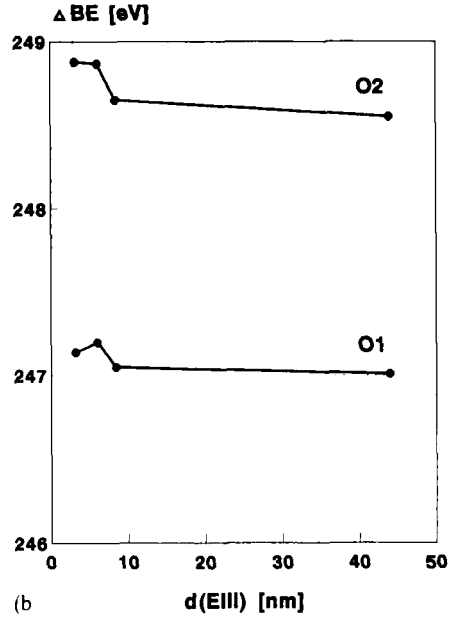

FIGURE 10 Relative binding energies for the components of C1s (a) and O1s (b) of PMMA on aluminium.

TABLE V
Relative intensity of the Cls components of PMMA on aluminium (240 W X-ray tube power)

d(Elli) [nm]	$\frac{C1}{C_{int}}$	$\frac{C3}{C4}$
3.0	0.569	1.041
3.1	0.630	1.154
6.0	0.517	0.984
8.4	0.438	1.018
44.0	0.457	1.023

values increase slightly for the C3 and C4 components in the thin films (cf. Fig. 10a). These BE shifts indicate a special polymer–substrate interaction on the natively oxidized aluminium.

In Figure 10b, the ether oxygen (O2) exhibits a significant rise in its ΔBE curve with decreasing polymer thickness. The carbonyl component O1 follows the same trend. As for the carbon in the methacryate groups, this ΔBE shift should be ascribed to a particular interphase interaction.

CONCLUSIONS

The detailed mathematical analysis of the various C1s and O1s photoelectron signals of PMMA films on gold and native aluminium oxide provides clear evidence for additional destruction processes not occurring in the polymer bulk. Two processes are found in the thin films on gold: the splitting of (—O—CH_3) units and the less pronounced stripping of complete methacrylate groups. On aluminium, only the second process has been verified. The intensity of these peculiar decomposition reactions rises in the vicinity of the phase boundary with the metal substrate. No such destruction mechanisms were observed in the thick bulklike layers. This latter result agrees with the statements in the literature[44-47] where depolymerization or backbone scission are reported as the dominating destructive processes even for AlK_α radiation (greater photon energy) and much higher flux densities than those applied in this work. In the bulk, it takes comparably longer radiation times to induce an additional separation of methacrylate groups.[46]

Hence, the two observed reactions of thermal destruction are considered as specific for the investigated polymer-metal interphases. Such additional low temperature destruction processes must be considered for the assessment of thermal stability of adhesive joints.

XPS does not allow for direct conclusions concerning path and products of the reaction. However, referring to the huge amount of oxygen bound on the aluminium surface, and to the strange absence of the "substrate oxygen" in the PMMA-gold interphase, it may be assumed that either the surface OH groups or the adsorbed water would be involved in those specific destruction reactions under the influence of the metal interface at elevated temperature. This hypothesis is illustrated by the following

schematic reaction equations:

$$CH_3—O\cdot + \cdot H \xrightarrow{\text{Au surface}} CH_3OH$$

$$CH_3—O—\underset{\underset{O}{\|}}{C}\cdot + \cdot OH \xrightarrow{\text{Au or Al surface}} CH_3OH + CO_2$$

It is well known from organic chemistry that the binding enthalpies, H, obey the relationship

$$H(C2\text{-}C4) < H(C4\text{-}O2) < H(O2\text{-}C3) \ll H(C4{=}O1)$$

in the methacrylate group of the PMMA (cf. Fig. 4). A specific environment such as the phase boundary to the metal could change this relationship to some extent, thus making the proposed reactions plausible.

Our hypothetic reaction scheme finds some similarity in mass spectroscopic investigations[48] of the thermal destruction of thin PMMA films on steel. In those experiments, methanol was detected as it evolved directly from the contact zone between steel and PMMA (radical polymerization) during the heating cycle, as long as the reservoir of adsorbed water on the steel was not exhausted. The surface-bonded water plays the decisive part on steel. Of course, this result cannot be transferred directly to the situation on Au or Al. But the XPS showed that the water adsorbed on the bare gold is no longer present beneath the PMMA layers. Thus, a certain similarity might exist to the findings on steel as far as the role of water is concerned.

These results and arguments favour a combination of mass spectrometry and XPS in future work. Mass spectrometry will not only provide direct information on the destruction products during the XPS measurements. At controlled sample temperature, these two techniques will open access to the simultaneous observation of destruction kinetics and specific interactions (in terms of bonding states) in polymer–metal interphases or polymer surface layers.

The presented experimental data reveal that only a small part of the methacrylate groups is involved in thermal destruction during the measurements. Most of the side groups remain intact and produce the photoelectron spectra expected for PMMA. No coupling between destruction and those complete side groups is resolved in the photo electron spectra.

Considering the influence on the binding energies in the PMMA molecule, the surfaces of gold and aluminium behave slightly differently. While on gold no changes of any of the polymer 1 s core levels have been detected in the interphase, there is a tiny shift of the 1 s binding energies for C3, C4, O1, and O2 towards higher values within a few nanometers distance to the aluminium substrate. The modification of the core level binding energies in the PMMA interphase to aluminium is not related to the special polymer destruction processes, because they occur on both metals. It has to be noted that the effects are quite weak. Each shift in binding energy by itself would not be enough to deduce an interphase interaction. But the combination of the several independent tendencies showing the same trend in the spectra supports our conclusion. Measurements on a spectrometer with improved energy resolution should be carried

out in the future to confirm the observed core level shifts in the PMMA interphase to oxidized Al.

Although XPS does not provide the answer for the causes of this energy shift on the native aluminium surface, one can speculate that the increase in core level binding energy is due to a partial reduction of electron density in the valence states. This depletion is possibly caused by a withdrawing force which the natively-oxidized aluminium exerts on the valence electrons of the PMMA side groups. As a very simple picture, the effect could be compared with the well-known behaviour of aluminium in complex chemistry. In distinction to gold, aluminium forms complex ions with water of the type

$$[Al\cdots OH\cdots H_2O]^{n+}$$

Such complexes are capable of acting as acceptors for the electrons of the methacrylate groups. This picture corresponds to the statements of the acid/base theory as well. So our experimental results confirm it for the PMMA – Al interphase.

The two special features deduced in this study for the interphase betwen PMMA and gold or aluminium demonstrate the benefit one can derive from application of XPS on a sophisticated level of experiment and data handling to the development of knowledge about solid interphases. Such information is of considerable value for the assessment of adhesion and stability of polymer–metal compounds. On the other hand, the discussion reveals once more the value of a combination of XPS and additional techniques. Concerning adhesion, core level XPS has the capability to provide indirect hints on strong interphase interactions. Deeper insight into this realm is expected from an interactive coupling of such measurements with appropriate quantum chemical modelling.

Acknowledgement

This study was supported in part by a grant from the Deutsche Forschungsgemeinschaft. This support is gratefully acknowledged by one of the authors (W.P.).

References

1. J. M. Burkstrand, *Surf. Sci.* **78,** 513 (1978).
2. J. M. Burkstrand, *Phys. Rev. B* **20,** 4853 (1979).
3. J. M. Burkstrand, *J. Appl. Phys.* **52,** 4795 (1981).
4. B. M. DeKoven and P. L. Hagans, *Applications Surf. Sci.* **27**, 199 (1986).
5. Lj. Atanasoska, S. G. Anderson, H. M. Meyer III, Zhangda Liu and J. H. Weaver, *J. Vac. Sci. Technol.* **A5,** 3325 (1987).
6. J. G. Clabes, M. J. Goldberg, A. Viehbeck and C. A. Kovac, *J. Vac. Sci. Technol.* **A6,** 985 (1988).
7. R. Haight, R. C. White, B. D. Silverman and P. S. Hp, *J. Vac. Sci. Technol.* **A6,** 2188 (1988).
8. L. J. Gerenser, *J. Vac. Sci. Technol.* **A8,** 3682 (1990).
9. P. Stoyanov, S. Akhter and J. M. White, *Surf. Interface Anal.* **15,** 509 (1990).
10. J. S. Solomon, D. Hanlin and N. T. McDevitt, in *Adhesion and Adsorption of Polymers*, L.-H. Lee, Ed., Vol. 12A of *Polymer Science and Techonology* (Plenum, New York, London, 1980), pp. 103–22.
11. J. Russat, *Surf. Interface Anal.* **11,** 414 (1988).
12. R. N. Lamb, J. Baxter, M. Grunze, C. W. Kong and W. N. Unertl, *Langmuir* **4,** 249 (1988).
13. S. P. Kowalczyk and J. L. Jordan-Sweet, *Chem. of Materials* **1,** 592 (1989).
14. S. A. Chambers, V. A. Loebs and K. K. Chakravorty, *J. Vac. Sci. Technol.* **A8,** 875 (1990).
15. W. Possart and W. Unger, in *Adhesion 15*, ed. by K. W. Allen Ed. (Elsevier Appl. Sci., London, New York, 1991), pp. 48–61.

16. A. P. Pijpers and W. A. B. Donners, *J. Polym. Sci.: Polym. Chem. Ed.* **23,** 453 (1985).
17. A. P. Pijpers and R. J. Meier, *J. Electr. Spectroscopy and Related Phenomena* **43,** 131 (1987).
18. R. J. Meier and A. P. Pijpers, *Theor. Chim. Acta* **75,** 261 (1989).
19. D. G. Castner and B. D. Ratner, *Surf. Interface Anal.* **15,** 479 (1990).
20. A. Naves de Brito, M. P. Keane, N. Correia, S. Svensson, U. Gelius and B. J. Lindberg, *Surf. Interface Anal.* **17,** 94 (1991).
21. G. Beamsom, A. Bunn and D. Briggs, *Surf. Interface Anal.* **17,** 105 (1991).
22. D.Fanter and W. Possart, *Fresenius J. Anal. Chem.* **344,** 199 (1992).
23. A.E. Hughes and B.A. Sexton, *J.Electr. Spectroscopy and Related Phenomena* **46,** 31 (1988).
24. A. Procter and D. M. Hercules, *Appl. Spectrosc.* **38,** 505 (1984).
25. ASTM Standards on Surface Analysis, ASTM Designation E 902–88, *Standard Practise for Checking the Operating Characteristics of X-Ray Photoelectron Spectrometers, in Surf. Interface Anal.* **17,** 889 (1991).
26. M. P. Seah, in *Practical Surface Analysis,* Vol. 1, *Auger and X-Ray Photoelectron Spectroscopy, 2nd. ed.,* D. Briggs and M. P. Seah, Eds (Wiley, Chichester 1990), chap.5, p. 245.
27. M. P. Seah, in *Practical Surface Analysis,* Vol. 1, *Auger and X-Ray Photoelectron Spectroscopy,* 2nd. ed., D. Briggs and M. P. Seah Eds. (Wiley, Chichester 1990).
28. M. S. McIntyre and T. C. Chan, in *Practical Surface Analysis,* Vol. 1, *Auger and X-Ray Photoelectron Spectroscopy,* 2nd. ed., D. Briggs and M. P. Seah Eds. (Wiley, Chichester 1990) Chap.5, p.501.
29. J. Stoch and L. Gablankowska-Kukucz, *Surf. Interface Anal.* **17,** 165 (1991).
30. S. A. Flodström, R. Z. Bachrach, R. S. Bauer and S. B. M. Hagström, *Phys. Rev. Lett.* **37,** 1282 (1976).
31. C. D. Wagner, W. M. Riggs, L. E. Davies, J. F. Moulder and G. E. Muilenberg, Eds., *Handbook of X-Ray Photoelectron Spectroscopy,* (Perkin-Elmer-Corp., Phys. Electr. Div., Eden Prairie, Minn., USA 1978) p. 50.
32. A.Fritsch and P. Legare, *Surf. Sci.* **186,** 247 (1987).
33. C. D. Wagner,in *Practical Surface Analysis,* Vol. 1, *Auger and X-Ray Photoelectron Spectroscopy,* 2nd. ed., D. Briggs and M. P. Seah, Eds. (Wiley, Chichester 1990) Chap.5, pp. 601–2.
34. B. R. Strohmeier, *Surf. Interface Anal.* **15,** 51 (1990).
35. I. Olefjord, H. J. Mathieu and P. Marcus, *Surf. Interface Anal.* **15,** 681 (1990).
36. H. E. Evans, W. M. Bowser and W. H. Weinberg, *Applications of Surf. Sci.* **5,** 258 (1980).
37. N. A. Thorne, P. Thuery, A. Frichet, P. Gimenez and A. Satre, *Surf. Interface Anal.* **16,** 236 (1990).
38. S. E. Bresler, A. T. Osminskaya, A. G. Popov, E. M. Saminskii and S. Ya. Frenkel', *Kolloidnij Zhurnal* **20,** 403 (1958).
39. R. J. Gritter, M.Seeger and D. E. Johnson, *J. Polym. Sci.: Polym. Chem. Ed.* **16,** 169(1978).
40. V. V. Korshak, *Uspekhi Khimii* **42,** 695 (1973).
41. H. H. G. Jellinek and M. D. Luh, *Makromol. Chem.* **115,** 89 (1968).
42. N. Grassie, in *Encyclopedia of Polymer Science and Technology,* Vol. 4 (Wiley & sons, New York, London, Sydney, 1966) pp. 647–716.
43. C. H. Bamford and C. F. H. Tipper, *Chemical Kinetics,* Vol. 14, *Degradation of Polymers* (Elsevier Sci. Publ., Amsterdam, Oxford, New York 1975) pp.10–24.
44. R. Chaney and G. Barth, *Fresenius Z. Anal. Chem.* **329,** 143 (1987).
45. E. M. Lehockey, I. Reid and I. Hill, *J. Vac. Sci. Technol.* **A6,** 2221 (1988).
46. E. M. Lehockey and I. Reid, *Surf. Interface Anal.* **11,** 302 (1988).
47. L. P. Buchwalter and G. Czornyi, *J. Vac. Sci. Technol.* **A8(2),** 781 (1990).
48. W.Possart, V. S. Yudin, B. P. Redkov, H.-J. Ziegler, O. F. Pozdnyakov and C. Bischof, *Acta Polymerica* **36,** 631 (1985).

APPENDIX: THE ROLE OF THE CONTAMINATION LAYER

The XPS spectra of the bare metal substrates revealed a carbon contamination of different constitution both on Au and Al. The thickness of these contamination layers is estimated from the XPS data in the following way.

For the integrated intensity I (*metal*) of the metal photo line beneath an overlayer (for example a contamination) of thickness, d_{ovl}, we have according to Ref. 26

$$I(\text{metal}) = I^{\infty}(\text{metal}) \exp\left[- \frac{d_{ovl}}{\delta_{ovl}(E_{metal}) \cdot \cos\theta} \right]$$

I^{∞}(metal) = integrated metal line intensity for a semi-infinite body
$\delta_{ovl}(E_{metal})$ = inelastic mean free path of the photo electrons from the metal in the overlayer
θ = collection angle of photo electrons with respect to the normal of the sample surface ("take-off angle")

The contamination overlayer provides a C1s intensity of

$$I(C1s) = I^{\infty}(C1s)\left\{1 - \exp\left[-\frac{d_{ovl}}{\delta_{ovl}(E_c)\cdot\cos\theta}\right]\right\} \tag{A2}$$

Further, the atomic sensitivity factors, S, due to Ref. 49, are applied:

$$\frac{I^{\infty}(\text{metal})}{I^{\infty}(C1s)} = \frac{S_{metal}}{S_C} \tag{A3}$$

Dividing (A1) by (A2) and introducing (A3) results in

$$\frac{I(\text{metal})}{I(\text{metal})}\frac{S(C1s)}{S(\text{metal})}\exp\left[-\frac{d_{ovl}}{\delta_C(E_{metal})}\right] + \exp\left[-\frac{d_{ovl}}{\delta_C(E_C)}\right] - 1 = 0 \tag{A4}$$

For organic materials, δ_C, the escape depth for the contamination layer, may be estimated from the equation[27]

$$\delta_C(E) = 49\cdot E^{-2} + 0.11\cdot E^{0.5} \tag{A5}$$

These equations (A4, A5) provide not only the thickness of the contamination, d_{cont}, on the bare metals that is calculated to be *ca.* 2.5 nm for Au and *ca.* 1.5 nm for Al. In addition, we can solve equation (A4) for all samples of PMMA layers where a metal line spectrum is obtained. The resulting d_{ovl} data correspond to the sum of the thickness values for the contamination and the polymer layers.

On the other hand, the ellipsometry provides a different thickness. The data for $d(Elli)$ are derived from two ellipsometric measurements prior to and after the formation of the PMMA layer. The contamination is included in the ellipsometric data for the bare metal and, therefore, $d(Elli)$ gives the actual thickness of the PMMA layer itself.

Hence, if the contamination layer would exist beneath the PMMA coating then we should always find

$$d_{ovl} \approx d(Elli) + d_{cont} \tag{A6}$$

The following Table compares the data obtained for the Al and the Au substrates

	Al; $d_{cont} \approx 1.5$ nm			Au; $d_{cont} \approx 2.5$ nm		
d_{ovl}[nm]	3.4	3.3	6	2.9	5.1	7.8
$d(Elli)$[nm]	3	3.1	4.8	3.4	4.6	8.2

The d_{ovl} data are less certain for the thicker layers since the intensity of the metal photo line decreases quickly with growing polymer thickness. However, in all cases we conclude from the data in the table that

$$d_{ovl} \approx d(Elli)$$

than the results according to equation (A6). This is a hint that the carbon contamination should not exist beneath the PMMA layers. Probably it dissolved and washed away during the process of coating with the polymer solution. Therefore, as a good approximation, the C1s signal for the polymer layers should stem only from the PMMA for the experiments described in this paper.